Photoelectron spectroscopic determination of the energy bandwidths of high-order harmonics (7th–55th) produced by an ultrafast laser in neon

Lora Nugent-Glandorf, Michael Scheer, M. Krishnamurthy,* Jennifer W. Odom, and Stephen R. Leone
JILA, National Institute of Standards and Technology and University of Colorado, Department of Chemistry and Biochemistry, Department of Physics, Boulder, Colorado 80309-0440
(Received 7 February 2000; published 20 July 2000)

The energy bandwidths of high-order harmonics of a Ti:sapphire ultrafast laser are extracted from electron kinetic-energy measurements of the photoionization of gas-phase atoms and molecules. High-order harmonics of the 70 fs, 800 nm laser are produced by focusing ≈ 2.5 mJ pulses into a jet of neon gas and are frequency-separated by a grazing-incidence grating. Photoelectrons resulting from the ionization of gaseous samples are energy-analyzed with a magnetic bottle time-of-flight spectrometer. Energy broadening of the photoelectron peaks at low kinetic energies are a direct result of the energy bandwidths of the harmonics. The energy bandwidths of the harmonics are found to increase from $0.11(\pm 0.03)$ eV (7th harmonic) to $0.37(\pm 0.03)$ eV (45th harmonic) in a gradual manner. The higher-order harmonics (47th–55th) appear to reach a plateau at a value of ≈ 0.43 eV. Though a full theoretical treatment of bandwidths of the harmonics for the 70 fs driving pulse regime does not exist, the theories developed for shorter pulses ($\leqslant 30$ fs) can give insight into the observed results.

PACS number(s): 42.65.Ky, 42.50.Hz, 32.80.Fb, 32.80.Rm

I. INTRODUCTION

The focusing of an intense ultrafast laser in a rare-gas medium provides a source of coherent, ultrafast vuv and soft-x-ray radiation via the nonlinear process of high-order harmonic generation (HHG). Since the first harmonic spectra were obtained in 1987 [1,2], an extensive amount of research has been done to understand the high-order harmonic generation process as well as the properties of the resulting vuv/soft x-ray light.

There are many unique characteristics of the harmonic generation process itself, which have been studied through both experiment and theory. It has been found that the extent of harmonic generation depends on several factors, such as the nature of the rare-gas medium, several aspects of the focusing conditions and spatial mode of the fundamental laser in the nonlinear medium [3], and the length and chirp of the fundamental pulse [4].

To a large extent, theory has successfully modeled these behaviors [5,6], and the basic process of generating high-order harmonics is well understood. A semiclassical model can qualitatively describe the harmonic generation process, in which the electron tunnels through the barrier formed by the Coulomb potential and the intense laser field. The electron then recombines with the parent atom upon reversal of the optical field, releasing coherent high-order radiation at odd harmonics of the fundamental wavelength [7]. However, the semiclassical model is unable to predict detailed spectral characteristics; hence, quantum models [8–10] are required for a more complete description.

In other nonlinear optical processes, such as third-order harmonic generation or four-wave mixing, it is possible to describe the electric field envelope of the generated light by introducing higher-order nonlinear electric susceptibilities of the medium, as perturbation theory suggests. In the case of high-order harmonic generation, however, small perturbations can no longer be used to describe the nonlinear process or the resulting pulse envelope. For example, it is not feasible to expand the susceptibility equation out to the 35th order. Similar arguments are made elsewhere in the literature [11].

A recent area of interest concerning the harmonics is the temporal and spectral characteristics of the generated soft-x-ray pulses. A great deal of literature has already been devoted to theoretical and experimental studies of the temporal width of the soft-x-ray pulses, most recently describing the exciting possibility of attosecond pulse generation [12,13]. It is known that for most experimental conditions the harmonic generation process favors the rising portion of the ultrafast laser pulse [4,14]. Pulse durations of the harmonics are predicted to be a factor of 3 shorter than the driving laser pulse length [8], and several experimental measurements confirm that the pulse length is indeed shortened, although the exact amount varies. For example, in Ref. [15], the pulse duration of the 23rd harmonic of a 70 fs Ti:sapphire laser was measured to be 50 ± 15 fs using a cross-correlation technique. In another experiment using a similar technique [16], the temporal width of the 19th harmonic of a Ti:sapphire laser was investigated as a function of the driving laser pulse length (120 fs–1 ps) and the position of the laser focus with respect to the gas jet. Although deconvolution of the width of the 19th harmonic was not possible, the cross-correlation full width at half maximum (FWHM) was always shorter than the driving laser pulse length.

A number of theoretical studies of the bandwidths of the harmonics of very short pulses ($\leqslant 30$ fs) are available [9,10]. According to calculations, both narrowing and broadening trends can exist with increasing harmonic number depending on the conditions of harmonic generation. In addi-

*Permanent address: Tata Institute of Fundamental Research, Homi Bhabha Road, Mumbai 400 005, India.

tion, studies of the intensity-dependent phase of the harmonics find an intrinsic blueshift and negative chirp. It is confirmed experimentally that for very short pulses the harmonic widths change dramatically as the fundamental pulse is positively or negatively chirped. In Ref. [14], discrete high-order harmonics are observed for positively chirped 25 fs excitation pulses where only continuous radiation is observed for the transform-limited and negatively chirped pulses. For longer driving laser pulses (≈ 100 fs), there are scattered experimental measurements of bandwidths of individual harmonics [17–19] (which will be summarized in Sec. III), but a systematic experimental investigation of the bandwidth vs harmonic number does not exist. In this work, we describe a method of directly measuring the spectral widths of a wide range of harmonics, in an attempt to provide new data to be tested by the existing theory and to complement previous measurements of the spectral profiles of ultrafast laser harmonics.

Quantum theoretical models can give spectral information when the particular conditions of an experiment are specified. Even so, quantum and numerical methods become increasingly difficult as the driving laser pulse length includes more optical cycles, and most of the existing theory is for pulses $\leqslant 30$ fs. Bandwidth measurements for harmonics produced by laser pulses in the intermediate range of 70 fs are therefore valuable since there is very little theoretical or experimental information available.

In addition to the importance of harmonic bandwidth to the theory of harmonic generation, bandwidth information is essential to consider the utility of the harmonics for time-resolved spectroscopy. The range of energies obtained by harmonic generation is ideal for spectroscopic studies of core levels in atoms and molecules. With a femtosecond source at these photon energies, many new possibilities arise, such as monitoring chemical shifts of core-level electrons for dissociating molecules in time. Pulses in the intermediate pulse duration range of 70 fs are expected to be well suited for pump-probe spectroscopy. Shorter pulses would produce harmonics that are spectrally too broad, and relevant spectroscopic structure would remain unresolved. Longer pulses produce harmonics that are spectrally narrow, but if the pulse duration becomes too long, the time scales for the processes that can be measured become limited and the harmonic efficiency decreases. It is also important to understand how the bandwidth changes with the harmonic number if one chooses to select different harmonics for photoionization.

The focus of the instrument described here is to eventually perform femtosecond x-ray photoelectron spectroscopy (FXPS) on molecular systems. Therefore, high photon flux in the individual harmonics, minimal bandwidth, and minimal chirp are important parameters. Although it is in principle possible to measure the bandwidths of the harmonics with high-resolution monochromators, the present work demonstrates that the energy bandwidths of the harmonics of a 70 fs Ti:sapphire laser system can alternatively be measured by using photoionization transitions in gaseous He, Ne, Kr, Xe, N_2, and NO. In this paper we describe the experimental apparatus used to collect valence shell and core-level photoelectron spectra of atoms and molecules with a femtosecond soft-x-ray light source. We use these photoelectron spectra to extract the spectral bandwidth of a wide range of harmonics with energies of $E_{h\nu}=15$–85 eV.

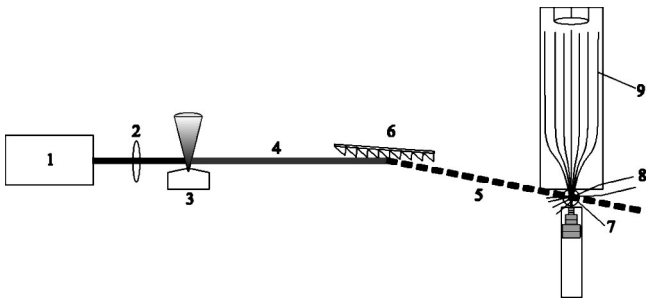

FIG. 1. Experimental apparatus. The output of a Ti:sapphire laser (1) is focused by a lens (2) into a rare-gas jet (3) to produce high-order harmonics of the laser (4). A single harmonic (5) can be selected with a grazing incidence grating (6) and focused into the interaction region (7) onto a gaseous sample (8). Electrons ejected from the sample gas are energy-analyzed with a magnetic bottle electron time-of-flight spectrometer (9).

II. EXPERIMENT

The experimental apparatus is shown in Fig. 1. An ultrafast laser is tightly focused into a rare-gas jet, where high-order harmonics of the laser (up to the 65th) are created. A single harmonic can be isolated with a grating and focused onto a gaseous sample (He, Ne, Kr, Xe, N_2, NO), where it causes photoionization. Electrons ejected from the sample gas are energy-analyzed using a magnetic bottle time-of-flight spectrometer.

The laser system consists of a seed Ti:sapphire oscillator, pumped by a frequency-doubled diode-pumped cw Nd:YVO_4 laser (532 nm), that generates 55 fs pulses centered at 800 nm. These pulses are then temporally stretched, subsequently seeded into a regenerative amplifier and a double-pass amplifier, where each stage is pumped by a frequency-doubled *Q*-switched Nd:YLF laser, and finally recompressed into femtosecond pulses. The final output of the laser system is 70 fs pulses at a 1 kHz repetition rate with $\leqslant 2.5$ mJ/pulse. This 1 cm diameter laser beam is tightly focused with a 45 cm lens (65 μm diameter spot size) into a neon gas jet. This yields a laser intensity in the jet of about 5×10^{14} W/cm^2. Harmonic generation occurs in the rare-gas medium, resulting in coherent radiation at the odd harmonics of the laser. We find that when the laser focus is located 2 mm after the center of the gas jet (confocal parameter $b \approx 30$ mm), maximum efficiency in the low-range to midrange harmonics is achieved, while moving the jet closer to the focus gives better signals in the higher harmonics (51st and above). All measurements reported here are taken with the laser focus after the gas jet, and data from the higher harmonics are compared at both laser focus positions (after the center of the jet and at the center of the jet). The 1 kHz rare-gas jet is produced with a piezocrystal behind a 1 mm nozzle, which is driven by 300 V square pulses synchronized to the 1 kHz repetition rate of the laser. The pulsed valve is backed by a Ne pressure of ≈ 280 kPa (40 psi) and pumped

by an 800 L/sec blower pump. The atomic density within the gas expansion at a distance of 1 mm (location of the laser beam) from the nozzle is $\sim 5\times 10^{17}$ atoms/cm^3.

A single harmonic can be selected from the resulting beam of vuv/soft-x-ray wavelengths utilizing a concave grating at grazing incidence (≈ 4 m radius of curvature, 1200 lines/mm, gold-coated). The grating is rotated about the center of its face using a commercial rotation stage with subdegree precision. The total angle between the entrance and exit beams is 150°. Since the beam is refocused to a line by the grating, we are able to select either a single harmonic in first order (9th to the 55th for these conditions) or all the harmonics in zeroth order (specular reflection), by a 0.5-mm-wide vertical slit located about 12 cm from the interaction region. The selected beam then enters the interaction region, which contains a sample gas of the atom or molecule under study.

Gaseous samples are introduced into the interaction region of the magnetic bottle spectrometer through a stainless-steel tube with a circular opening of approximately 0.3 mm in diameter. A leak valve controls the continuous flow of the gas going through the opening. The chamber pressure rises from a base pressure of 6.7×10^{-6} Pa (5×10^{-8} Torr) to between 6.7×10^{-4} and 1.3×10^{-2} Pa (5×10^{-6} and 1×10^{-4} Torr) during experiments.

In the interaction region where the harmonic beam and particle beam cross, photoionization occurs and the resulting photoelectrons are collected into a magnetic bottle time-of-flight electron analyzer. The electrons are captured by a high magnetic field (≈ 7.4 kG) in the interaction region, produced by a stack of SmCo permanent magnets approximately 2.5 cm below the sample gas inlet. The ≈ 1.4 m flight tube is differentially pumped relative to the interaction region (to maintain pressures below 1×10^{-4} Pa or 1×10^{-6} Torr) and is wrapped with a wire coil through which a 3 A dc current is passed to create a low magnetic field (see field lines in Fig. 1). This magnetic-field configuration serves to ensure a high collection efficiency of electrons over a large angle of initial trajectories (2π steradians) [20]. All parts within the interaction region are coated with graphite to minimize surface charging and contact potential effects. Pairs of retarding grids are placed at each end of the flight tube to decelerate electrons up to -40 V, while maintaining an electrically field-free region in the flight tube. This allows us to isolate any region of a spectrum and bring it below 5 eV photoelectron energy where the resolution of the spectrometer is optimal. A microchannel plate detector is used to detect the electrons arriving in real time. The preamplified detector pulses are analyzed with a multichannel scaler with 5 ns bin resolution. A quadrupole mass spectrometer is located opposite to the gas jet to allow for photoion mass analysis when necessary, but was not used in this study.

III. RESULTS AND DISCUSSION

To calibrate the resolution of the magnetic bottle time-of-flight spectrometer, a narrow bandwidth laser source was used to photoionize NO gas. The ninth harmonic of 1064 nm (118 nm) was created by focusing the standard 355 nm output (third harmonic) of a commercial Nd:YAG laser into a static cell of Xe gas at 3 torr. The 118 nm output (10.5 eV) was used to ionize NO slightly above threshold (9.26 eV [21]), giving low-energy photoelectron peaks (below 2 eV). This spectrum is shown as the dashed line in Fig. 2. Vibrational resolution is achieved in the NO^+ X state, and photoelectrons resulting from $v=0$, 1, and 2 are observed. In this way, an energy calibration of the magnetic bottle spectrometer was obtained at low energies, and the inherent resolution of the system was determined.

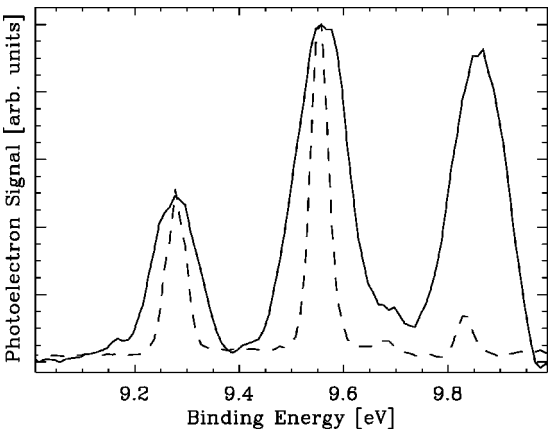

FIG. 2. Photoelectron spectrum of NO gas taken with the 9th harmonic of a long pulse, narrow band Nd:YAG laser, $E_{h\nu}=10.496$ eV (dashed line). Here the inherent resolution of the magnetic bottle spectrometer is seen in the peak widths. The vibrational progression of the NO^+ ground state gives rise to the three peaks separated by ≈ 0.28 eV. The solid line shows the same vibrational progression, but with the 7th harmonic (centered at $E_{h\nu}=10.91$ eV) of the fs Ti:sapphire laser. The broadening of the peaks is due to the energy bandwidth of the 7th harmonic. The height discrepancy in the highest binding-energy peak between the Nd:YAG laser and the 7th harmonic of the Ti:sapphire laser is due to the efficiency of the photoelectron spectrometer at different photoelectron energies. Though these peaks have the same binding energy, the dashed line peak corresponds to very low photoelectron energy, where the collection efficiency is quite low.

The bandwidth of the NO photoelectron peaks using the nanosecond laser is limited by the resolution of the spectrometer and not by the narrow bandwidth of the laser. The best reported magnetic bottle resolution is $\Delta E_{pe}/E_{pe}\approx 1\%$ [20], when the magnetic fields are meticulously adjusted. The $\Delta E_{pe}/E_{pe}$ of our NO data was found to be $\approx 5\%$, giving the basic resolution for the magnetic bottle spectrometer. Here and throughout the paper, E_{pe} designates photoelectron energy and $E_{h\nu}$ represents photon energy. The $\Delta E_{pe}/E_{pe}$ for any magnetic bottle system is approximately a constant number with E_{pe} [20], therefore limiting the useful energy range over which bandwidth information of the light source can be obtained. For example, for a $\Delta E_{pe}/E_{pe}$ of 5% there is already a spectrometer broadening of 0.25 eV at a photoelectron energy of 5 eV. Therefore, for photoelectron peaks at energies beyond 5 eV, a broadening due to the energy bandwidth of the photon source that is less than 0.25 eV is masked by the spectrometer resolution. This means that unambiguous bandwidth information can only be extracted from low-energy photoelectron peaks. In this work, two

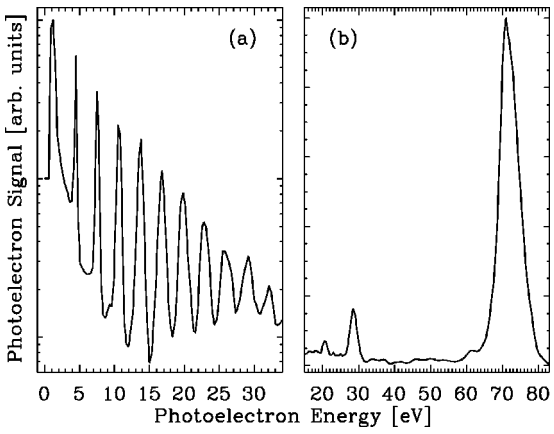

FIG. 3. (a) Photoelectron spectrum due to all harmonics simultaneously incident on a sample of He gas. The first harmonic energetic enough to ionize He is the 17th ($E_{h\nu}=26.4$ eV). Each subsequent harmonic is seen as another main ionization peak at increasingly higher energies. (b) A single harmonic (61st, $E_{h\nu}=95$ eV), selected by the grazing incidence grating incident on a sample of He gas. Not only is the main ionization peak seen, but also the first and second satellite peaks.

methods are therefore utilized. Specific atomic or molecular transitions that fortuitously yield low-energy electrons for certain harmonics are studied in one series of measurements and the retarding grids are used to lower the electron energies in the other.

After determining the magnetic bottle resolution, the harmonics from the Ti:sapphire laser are used to produce photoionization spectra. When light from the zeroth-order diffraction of the grating, the specular reflection, is incident upon a sample of helium gas, the photoelectron spectrum in Fig. 3(a) is obtained. The first harmonic to ionize He is the 17th (26.35 eV), and each higher harmonic ionizes He as well, giving a harmonic spectrum. Up to the 37th harmonic, the spectrum is clearly resolved. As can be seen, the resolution of the data-acquisition system is quite good at low photoelectron energies, is limited by the magnetic bottle resolution in the mid-energy range as discussed above, and finally is further limited by the 5 ns bins of the multichannel scaler in the high-energy range.

By rotating the grating away from the specular reflection, single harmonics can be selected. Figure 3(b) shows the photoelectron spectrum that results from a single harmonic incident on He, in this case the 61st. Not only do we observe the main photoionization peak, but also the first and second satellite peaks. The binding energy and the cross sections of the He main and satellite peaks are well known [22], and from this we are able to calculate the photon flux present in a single harmonic. For the high-order harmonics within the plateau region (41st to 61st with Ne as nonlinear medium), we estimate, to an order of magnitude, that $\sim 10^5$ photons/pulse in an individual harmonic actually reach the interaction region, or $\sim 10^8$ photons/sec with the 1 kHz repetition rate laser. There is severe astigmatism associated with using a concave grating at grazing incidence, and the harmonics focus to a line instead of a spot. The beam is apertured with an iris, resulting in a significant reduction of the photon flux. These losses considered, the photon flux is in agreement with high-order harmonic photon fluxes reported elsewhere with similar systems [23,24].

By compiling the He data for the various harmonics, a calibration of the magnetic bottle spectrometer over the full kinetic energy range is made. A plot of the known photoelectron energy, $E_{pe}=E_{h\nu}-I_p$, vs time-of-flight of the electrons, t, is expected to follow the equation

$$E_{pe}=\frac{1}{2}m_e\left(\frac{d}{t}\right)^2, \tag{1}$$

where m_e is the mass of the electron and d is the distance traveled by the electron. To fit the acquired data to a proper t^{-2} curve, both a time and energy offset are introduced, and Eq. (1) becomes

$$E_{pe}=E_0+\frac{1}{2}m_e\left(\frac{d}{(t+t_0)}\right)^2. \tag{2}$$

By allowing d, t_0, and E_0 to be variables, a nearly perfect fit to the data is obtained, giving values of $d=1.38(\pm 0.04)$ m, $t_0=-0.03(\pm 0.01)$ μs, and $E_0=0.16(\pm 0.15)$ eV. The flight tube distance agrees well with the physical dimensions of the system, and the t_0 offset is due to the inherent delay between the arrival of the laser pulse at the interaction region and the trigger signal derived from a photodiode. Based on the uncertainties of the calibration parameters, we estimate the uncertainty in the bandwidth measurements to be ± 0.03 eV.

High-order harmonics may exhibit a blueshift due to the intensity-dependent phase of the harmonic generation process. For very short pulses ($\leqslant 25$ fs), the amount of blueshift can change with harmonic number, due to the very fast intensity variation of the optical driving pulse. In our case, with a 70 fs pulse, harmonic generation occurs predominantly during the rising edge and peak of the driving pulse, thus the variation of the pulse intensity can be considered approximately linear in time, giving a constant blueshift [25] for all harmonics. However, the E_0 offset for our calibration is nearly zero within the uncertainty. It is conceivable that a very small contact potential effect in the interaction region, despite the graphite coating, and a small constant blueshift of the harmonics compensate each other.

After proper calibration of the spectrometer, photoelectron spectra of several atomic and molecular gases were taken, using either the specular reflection of the grating or individual harmonics. From these photoelectron spectra, we measured photoelectron peaks resulting from ionization of a number of different harmonics. First, by using several different target gases, it is possible to obtain low-energy photoelectron peaks directly resulting from ionization with a range of harmonics. Each atom or molecule has a characteristic ionization potential and precise core-level binding energies. Sample spectra using Xe as the target gas are shown in Fig. 4. The line doublet shown in Fig. 4(a) results from ionization from the $5p_{1/2}$, and $5p_{3/2}$ valence levels with the 11th harmonic, whereas the doublet in Fig. 4(b) is due to ionization from the $4d_{3/2}$ and $4d_{5/2}$ core levels with the 47th harmonic.

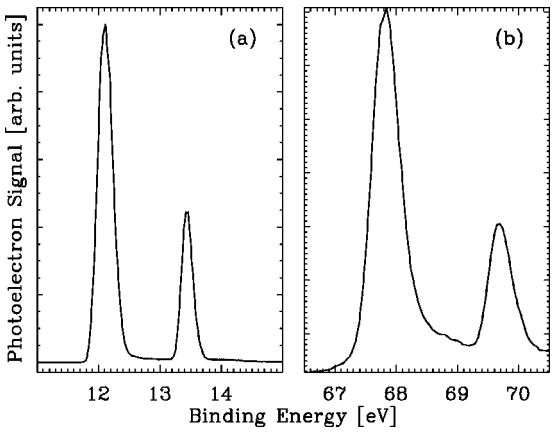

FIG. 4. Photoelectron spectra of Xe using single harmonics: (a) ionization from $5p$ valence levels by the 11th harmonic; (b) ionization from $4d$ core levels by the 47th harmonic.

This figure demonstrates the wide range of photon energies available, with which we are able to obtain both valence and core photoelectron spectra with good resolution.

Photoelectron spectra of Ne, Ar, and Kr were also taken. Similar to Xe, the main ionization peaks of these other rare gases exhibit a doublet structure due to the fine-structure splitting of the ionic ground state. This splitting is too small in the cases of Ne and Ar to be fully resolved and the corresponding peaks were not used for bandwidth measurements. Ionization of rare gases from ns levels, on the other hand, does not suffer from fine-structure splitting, but the cross sections are generally small. This ionization process was only observed in the case of Ne.

Photoelectron spectroscopy of molecular gases with the harmonics is also possible, and several peaks from N_2 and NO were measured. The peaks from NO, shown as the solid line in Fig. 2, are especially important, since they represent the same vibrational progression that was obtained with the narrow band Nd:YAG laser, except using the 7th harmonic of the Ti:sapphire laser. Comparison of the two spectra in Fig. 2 clearly shows the broadening of the photoelectron peaks due to the bandwidth of the 7th harmonic.

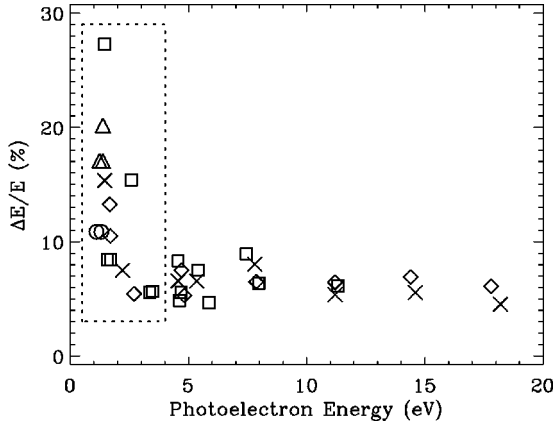

FIG. 5. The relative energy width of photoelectron peaks from several different gases vs their respective photoelectron energies. The higher-energy photoelectron peaks converge to a relative width of 4–5 %. For photoelectron peaks below ≈ 4 eV, a new trend can be seen, where the ΔE of the peaks is due to the energy bandwidth of the harmonics. Target gas is He ($\diamond$), Ne ($\times$), Xe ($\square$), N_2 ($\triangle$), and NO ($\bigcirc$).

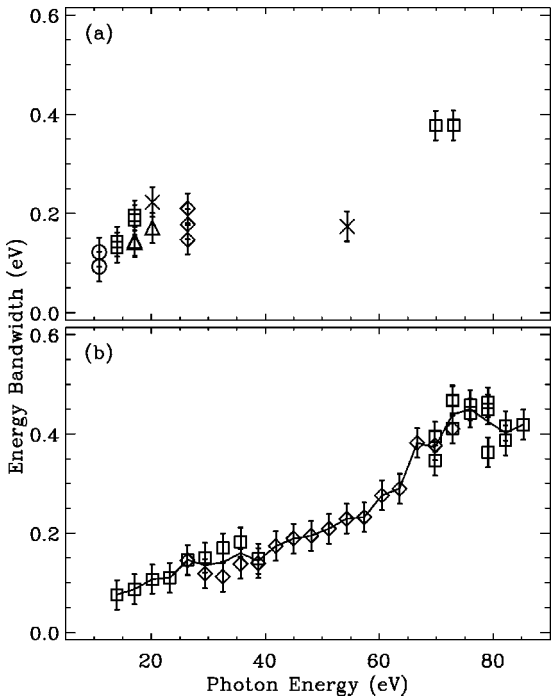

FIG. 6. (a) The absolute energy width of the low-energy photoelectron peaks from Fig. 5 (below 4 eV) is plotted as a function of the photon energy or the harmonic used to ionize the electron from which the peak arises. The retarding grids in the electron flight tube were not used for this data set. (b) A more complete data set using the retarding grids to measure the bandwidths of all the harmonics from the 9th to the 55th. Comparison of (a) and (b) shows that no artificial broadening exists when utilizing the retarding grids. Target gas is He ($\diamond$), Ne ($\times$), Xe ($\square$), N_2 ($\triangle$), and NO ($\bigcirc$), and the solid line is the average for each harmonic.

Using all the data discussed above from He, Kr, Xe, N_2, and NO, we measured the full width at half maximum of several photoelectron peaks with energies ranging from 1 to 20 eV. In Fig. 5, a plot of $\Delta E_{pe}/E_{pe}$ vs photoelectron energy, E_{pe}, is shown. From this figure two different trends in measured bandwidth can be seen. The high kinetic energy photoelectron peaks converge to a value around 5%, which is due to the spectrometer resolution, and the peaks below ≈ 4 eV photoelectron energy show a steep rise, where the bandwidth is primarily due to the energy width of the harmonic light used to eject that electron. We then take the points below 4 eV in Fig. 5 and, after deconvolution with the spectrometer width, plot ΔE_{pe} (now equal to $\Delta E_{h\nu}$) as a function of photon energy, $E_{h\nu}$, in Fig. 6(a). All the points in Fig. 6(a) were taken without the use of the retarding grids.

A more complete study was done, however, by utilizing the retarding grids in the magnetic bottle system. In this way, a particular transition (for example, the main ionization peak of He) can be selected, and the electron kinetic energy shifted into the region where the bandwidth of the laser dominates the spectrometer width for each harmonic (under

TABLE I. A tabulation of the average energy widths for all harmonics from the 7th to the 55th as taken from Fig. 6 (uncertainty is ± 0.03 eV).

Harmonic	ΔE (eV)	Harmonic	ΔE (eV)
7	0.11	33	0.21
9	0.08	35	0.23
11	0.09	37	0.22
13	0.10	39	0.28
15	0.11	41	0.29
17	0.15	43	0.38
19	0.14	45	0.37
21	0.14	47	0.44
23	0.16	49	0.45
25	0.14	51	0.43
27	0.17	53	0.40
29	0.19	55	0.42
31	0.20		

3 eV photoelectron kinetic energy after deceleration). Figure 6(b) shows $\Delta E_{h\nu}$ vs $E_{h\nu}$ for the measured bandwidths of all harmonics from the 9th to the 55th using the main ionization line in He and the $Xe \rightarrow Xe^{+}(5p_{3/2}^{-1})$ and $Xe \rightarrow Xe^{+}(4d_{5/2}^{-1})$ transitions. It can be seen from comparison of the two plots in Fig. 6 that the general trend is very similar, which gives confirmation that any broadening effect of the retarding grids can be ruled out. A list of the average $\Delta E_{h\nu}$ values for harmonics 9–55 are listed in Table I.

In Fig. 6, the natural widths of the Xe $4d$ core-level peaks are taken into account. Core-level ionization results in an ionic core-hole state that decays very rapidly via Auger processes. Hence, core-level photoelectron peaks may exhibit a significant natural linewidth. The width of the Xe $4d$ levels has been the subject of several previous investigations, which report widths between 0.10 and 0.12 eV [26,27]. The measured widths of the Xe $4d$ peaks in Fig. 6 and Table I are corrected for both the spectrometer broadening and the natural linewidth.

The dominant source of chirp and thus temporal broadening of the high-order harmonics stems from the harmonic generation process itself. It has been reported that an unchirped driving pulse produces negatively chirped harmonics and that the best high-order harmonic generation is achieved if the driving pulse is slightly positively chirped [14]. We have investigated the effect of a chirped fundamental pulse on the high-order harmonic photoelectron spectra for both positive and negative chirps of up to 0.3 nm/fs. While for small positive chirps of ≈ 0.1 nm/fs the harmonic generation efficiency is slightly improved compared to an unchirped driving pulse, the efficiency drops off strongly for more positively and for negatively chirped pulses. The measured bandwidths, however, remain constant except for large negative chirps where a broadening of about a factor of 1.5 was observed.

In the present setup, the monochromator grating constitutes another source of chirp for the harmonic pulses. It is well known that a grating introduces a certain amount of chirp to an ultrafast optical pulse, due to the phase dispersion of the grating. We have investigated the effect of this chirp on the bandwidth of the harmonic pulses experimentally by comparing a photoelectron peak obtained with a single harmonic with the identical peak obtained with the specular reflection. In the latter case no chirp is introduced, since the grating is being used only as a mirror. No difference was found between the widths of the respective peaks indicating that there is only minimal effect of the grating on the bandwidth. However, in the context of pump-probe experiments, a purely temporal broadening of the high-order harmonic pulses would still be of concern. A grazing incidence grating introduces a temporal broadening due to both phase front tilt and angular dispersion [28]. Depending on the area of the grating that is illuminated by the high-order harmonic pulse, a temporal stretching of several hundred femtoseconds may occur. The possibility of minimizing this effect with a two-grating setup is currently being evaluated.

In one experiment with similar conditions to the system here, a narrow slit monochromator is used to scan through the 27th harmonic of a 140 fs Cr:LiSAF laser. The energy bandwidth of the 27th harmonic is found to be ≈ 0.12 eV [17]. This agrees well with the result from this work (0.17 eV for the 27th harmonic), because a slightly larger energy bandwidth is expected here corresponding to our shorter pulse length. In another experiment, the 7th and 9th harmonics of a 100 fs Ti:saphhire laser are measured to have a FWHM of ≈ 0.1 eV [19], also consistent with the measurements here. Measured bandwidths of harmonics generated by picosecond lasers, such as in Ref. [18], are quite narrow and cannot be compared directly to the results found here. Though other harmonic spectra are reported throughout the literature [3,4,29,30], bandwidth measurements are not discussed and are not easily derived from the figures.

The general trend seen in Fig. 6 is a gradually increasing bandwidth from the 7th harmonic to the 45th harmonic, from $0.11(\pm 0.03)$ eV to $0.37(\pm 0.03)$ eV. The higher harmonics, from the 47th–55th, seem to reach a plateau centered around 0.43 eV. Theoretical treatments of spectral width vs harmonic number do exist for driving laser pulses $\leqslant 30$ fs [8,9]. Comparison of the results reported here and these theoretical predictions is difficult for several reasons. First, for longer driving laser pulses, theory becomes increasingly difficult as more optical cycles must be treated numerically. Second, for very short pulses, saturation due to ionization of the nonlinear gas medium is not reached, since the response time of the atoms is slow compared to the temporal envelope of the pulse. In the case of longer pulses, however, saturation is reached somewhere after the peak of the pulse on the falling edge. Nevertheless, we believe it is beneficial to mention the results of theoretical calculations and draw comparisons where it is appropriate.

According to calculations in the single atom picture of harmonic generation from short pulses, the phase structure of the generated harmonics plays a significant role [8]. A simple quadratic phase structure gives rise to linear chirp in the pulse, and no broadening of the spectrum within the pulse occurs. On the other hand, a complex phase structure with higher-order terms leads to nonlinear chirp and thus

broadening of the spectrum through the introduction of new spectral components. The phase of the generated harmonics is said to be dependent on the intensity variation of the driving pulse, which changes dramatically during harmonic generation for a very short pulse. In this single atom picture, the lower-range and midrange harmonics have a complex phase structure, due to the fact that these harmonics are created over a larger number of optical cycles, with contributions from the rising edge, the peak, and the falling edge of the pulse. The higher harmonics near the cutoff, however, are created over the few optical cycles near the peak of the pulse, giving rise to a simple quadratic phase structure. This leads to calculated harmonic spectra with broad, unresolved lower harmonics and well-resolved harmonics near the cutoff.

However, when the macroscopic conditions of harmonic generation are considered in addition to the single atom response, the results can be much different. In Ref. [9], several aspects of the bulk medium are considered, such as phase matching and the focus position of the laser with respect to the gas jet. They give a two-trajectory picture of harmonic generation, where the ionized electron can return to the ion on a short or long trajectory. These two trajectories can interfere with each other, or one can dominate depending on the conditions of harmonic generation. If the jet is located after the focus, the short return time is dominant, which results in a weak intensity dependence of the phase. This gives rise to a well-resolved spectrum with decreasing widths for decreasing harmonics orders. If the jet is at the focus, the calculated spectrum shows the opposite trend.

The argument that the high-order harmonics near the cutoff are created only near the peak of the driving pulse is expected to remain true for 70 fs pulses. Therefore, it could be argued that the plateau seen in Fig. 6(b) is due to this effect, namely that the harmonics in the cutoff region exhibit only a constant linear chirp and no further broadening is seen. It may seem that the two-trajectory picture could account for the fact that we see a decreasing bandwidth with decreasing harmonic number, but we do not observe any difference in the bandwidths of the high-order harmonics when the position of the jet with respect to the focus is changed. We therefore conclude that a theoretical study based on the particular parameters of this experiment is needed to fully explain the observed bandwidth trends.

IV. CONCLUSION

In this work, we report the energy bandwidth of a range of harmonics from the 7th to the 55th of a 70 fs Ti:sapphire laser. The bandwidths of the 7th to the 45th harmonics increase gradually from $0.11(\pm 0.03)$ to $0.37(\pm 0.03)$ eV, and reach a plateau of ≈ 0.43 eV from the 47th to the 55th harmonics. To our knowledge, the results given here constitute the first systematic experimental study of spectral bandwidths for an intermediate pulse duration. We have shown that these harmonics can indeed be useful for future time-resolved spectroscopic studies.

ACKNOWLEDGMENTS

We would like to acknowledge funding from the U.S. Air Force Office of Scientific Research and additional equipment from the National Institute of Standards and Technology and the National Science Foundation. We would also like to acknowledge Tobias Voss for his contribution in characterizing the chirp of the ultrafast laser pulses. L.N.-G. recognizes support from the Optical Science and Engineering Program, funded by the National Science Foundation through its IGERT initiative. M.S. would like to acknowledge support from the Natural Sciences and Engineering Research Council of Canada.

[1] M. Ferray, A. L'Hullier, X.F. Li, L.A. Lompre, G. Manifray, and C. Manus, J. Phys. B **21**, L31 (1988).
[2] A. McPherson, G. Gibson, H. Jara, U. Johann, T.S. Luk, I. McIntyre, K. Boyer, and C.K. Rhodes, J. Opt. Soc. Am. B **4**, 595 (1987).
[3] C.G. Wahlstrom, J. Larsson, A. Persson, T. Starczewski, S. Svanberg, P. Salieries, P. Balcou, and A. L'Huillier, Phys. Rev. A **48**, 4709 (1993).
[4] J. Zhou, J. Peatross, M.M. Murnane, H.C. Kapteyn, and I.P. Christov, Phys. Rev. Lett. **76**, 752 (1996).
[5] M. Lewenstein, Ph. Balcou, M.Yu. Ivanov, A. L'Huillier, and P.B. Corkum, Phys. Rev. A **49**, 2117 (1994).
[6] A. Sanpera, J.B. Watson, M. Lewenstein, and K. Burnett, Phys. Rev. A **54**, 4320 (1996).
[7] P.B. Corkum, Phys. Rev. Lett. **71**, 1994 (1993).
[8] K.J. Schafer and K.C. Kulander, Phys. Rev. Lett. **78**, 638 (1997).
[9] P. Salieres, P. Antoine, A. de Bohan, and M. Lewenstein, Phys. Rev. Lett. **81**, 5544 (1998).
[10] C. Kan, C.E. Capjack, R. Rankin, and N.H. Burnett, Phys. Rev. A **52**, R4336 (1995).
[11] J.L. Krause, K.J. Schafer, and K.C. Kulander, Phys. Rev. A **45**, 4998 (1992).
[12] N.H. Shon, A. Suda, and K. Midorikawa, Phys. Rev. A **60**, 2587 (1999).
[13] V.T. Platonenko and V.V. Strelkov, Quantum Electron. **28**, 749 (1998).
[14] Z. Chang, A. Rundquist, H. Wang, I. Christov, H.C. Kapteyn, and M.M. Murnane, Phys. Rev. A **58**, R30 (1998).
[15] T.E. Glover, R.W. Schoenlein, A.H. Chin, and C.V. Shank, Phys. Rev. Lett. **76**, 2468 (1996).
[16] A. Bouhal, P. Salieres, P. Breger, P. Agostini, G. Hamoniaux, A. Mysyrowicz, A. Antonetti, R. Constantinescu, and H.G. Muller, Phys. Rev. A **58**, 389 (1998).
[17] Ph. Balcou, P. Salieres, K.S. Budil, T. Ditmire, M.D. Perry, and A. L'Huillier, Z. Phys. D: At., Mol. Clusters **34**, 107 (1995).
[18] J. Larsson, E. Mevel, R. Zerne, A. L'Hullier, C.G. Wahlstrom, and S. Svanberg, J. Phys. B **28**, L53 (1995).
[19] C. de Lisio, C. Altucci, R. Bruzzese, F. De Filippo, S. Solimen, M. Bellini, and P. Foggi, Appl. Phys. B: Lasers Opt. **64**, 323 (1997).

[20] P. Kruit and F.H. Read, J. Phys. E **16**, 313 (1983).
[21] D.W. Turner, *Molecular Photoelectron Spectroscopy* (John Wiley and Sons, New York, 1970), p. 54.
[22] S. Svensson, A. Kikas, A. Ausmees, S.J. Osborne, S. Aksela, A. Naves de Brito, and E. Nommiste, J. Phys. B **28**, L293 (1995).
[23] R. Haight, Appl. Opt. **35**, 6445 (1996).
[24] T. Ditmire, J.K. Crane, H. Nguyen, L.B. DaSilva, and M.D. Perry, Phys. Rev. A **51**, R902 (1995).
[25] J.B. Watson, A. Sanpera, and K. Burnett, Phys. Rev. A **51**, 1458 (1995).
[26] S. Masui, E. Shigemasa, A. Yagishita, and I.A Sellin, J. Phys. B **28**, 4529 (1995).
[27] A. Ausmees, S.J. Osborne, R. Moberg, S. Svensson, S. Aksela, O.-P. Sairanen, A. Kivimaki, A. Naves de Brito, E. Nommiste, J. Jauhiainen, and H. Aksela, Phys. Rev. A **51**, 855 (1995).
[28] J.C. Diels and W. Rudolph, *Ultrashort Laser Pulse Phenomena* (Academic Press, San Diego, 1996).
[29] A. L'Huillier, M. Lewenstien, Ph. Balcou, P. Salieres, M.Y. Ivanov, J. Larsson, and C.-G. Wahlstrom, Phys. Rev. A **48**, R3433 (1993).
[30] C. Altucci, C. Delfin, L. Roos, M.B. Gaarde, A. L'Huillier, I. Mercer, T. Starzewski, and C.-G. Wahlstrom, Phys. Rev. A **58**, 3934 (1998).